THE ASTRONOMICAL JOURNAL, 120:3201–3217, 2000 December

WIND INHOMOGENEITIES IN WOLF-RAYET STARS. IV. USING CLUMPS TO PROBE THE WIND STRUCTURE IN THE WC8 STAR HD 192103

SÉBASTIEN LÉPINE,[1] ANTHONY F. J. MOFFAT,[2,3,4] NICOLE ST-LOUIS,[2,3] SERGEY V. MARCHENKO,[2] MATTHEW J. DALTON,[5] PAUL A. CROWTHER,[5,6] LINDA J. SMITH,[5] ALLAN J. WILLIS,[5] IGOR I. ANTOKHIN,[7] AND GAGHIK H. TOVMASSIAN[8]

Received 2000 June 14; accepted 2000 August 16

ABSTRACT

We present the most intensive, high-quality spectroscopic monitoring of optical Wolf-Rayet emission lines ever obtained. The Wolf-Rayet star HD 192103 (=WR 135; subtype WC8) was observed in the 5650–5840 Å regime alternately from both the William Herschel Telescope and the Canada-France-Hawaii Telescope. The final data consist of a series of 197 spectra spread over 64 hr, each with a resolving power $\lambda/\Delta\lambda \simeq 20{,}000$ and a signal-to-noise ratio in the continuum $\simeq 450$ per 3 pixel resolution element. We clearly and unambiguously identify stochastic, structured patterns of intrinsic variability at the 1%–2% level of the line flux in the broad C III λ5696 emission line. The λ5801/12 doublet emission is also found to be variable at the 0.2%–0.5% level of the line flux. We find a correlation between the variability patterns observed in C III and C IV, which suggests a significant overlap in the emission volumes of these transitions, although C IV is known to arise somewhat closer to the star. We attempt to reproduce the observed line profile variation patterns using a simple phenomenological model, which assumes the wind to be fully clumped. With a minimal set of assumptions, we are able to reproduce both the shape and the variability in the C III λ5696 emission profile. We show that the variability pattern provides constraints on the radial extent of WR 135's wind where C III is produced, as well as on the local wind acceleration rate. However, our simple clump model does not reproduce the lower variability in the C IV doublet unless we assume the C IV emission to occur in a much larger volume than C III, implying that significant C IV emission occurs farther out in the wind than C III. We suggest that while some C IV emission might occur farther out, possibly because of reionization from shocks, a more likely explanation is that wind clumping significantly increases with distance from the star, leading to larger variability levels in C III, formed farther out than most of C IV. Alternatively, optical depth effects and/or local ionization gradients within clumps could conspire to attenuate clumping effects in the C IV emission line while enhancing them in the C III line.

Key words: stars: emission-line, Be — stars: individual (HD 192103) — stars: Wolf-Rayet

1. INTRODUCTION

Wolf-Rayet (WR) stars are evolved objects characterized by intense mass-loss in the form of a dense, fast wind, typically resulting in a $\dot{M} \approx 10^{-5}\ M_\odot\ \mathrm{yr}^{-1}$ net outflow accelerated to a high $v_\infty \approx 2000$ km s^{-1} terminal velocity. WR stars are characterized by very broad emission lines of heavy elements (mainly N for WN subtypes, and C, O for WC subtypes), in addition to He in both subtypes and sometimes H in WN subtypes. Some emission lines are flanked by a blueward P Cygni absorption component, typical of dense stellar winds.

Theoretical models of WR atmospheres have traditionally relied on a set of simplifying hypotheses within the framework of a so-called standard model (SM). In the SM, the wind is assumed to be steady, homogeneous, and spherically symmetric (see, e.g., Hamann et al. 1992). However, the SM has failed to explain an increasing number of observational characteristics, all of which suggest that the wind is neither steady nor homogeneous and sometimes not even spherically symmetric. Hillier (1991) showed that the electron scattering wings, which flank the red sides of WR wind emission lines, are observed to be systematically weaker than predicted by the SM. Recombination line emission is locally proportional to the square of the density, whereas electron scattering is directly proportional to the overall wind density. Thus, relatively weaker electron scattering wings can be expected if there are local overdensities in the wind, i.e., if the wind is clumped (Hamann & Koesterke 1998).

The slope and shape of the infrared and radio continua from WR stars also provide strong evidence for wind clumping. The SED spectral index $\alpha[S_\nu \sim \nu^\alpha]$ in the millimeter-to-centimeter wavelength regime is larger than predicted from free-free emission models of steady, homogeneous winds (Nugis 1994). In addition, the observed continuum X-ray emission is explained by the presence of an ultrahot component, possibly arising in wind material compressed by shocks (Maeda et al. 1999).

One of the main consequences of wind clumping is the reduction of mass-loss rates as estimated from recombination-line spectral analyses or from radio/IR continuum measurements. Nugis, Crowther, & Willis (1998)

[1] Department of Astrophysics, American Museum of Natural History, Central Park West at 79th Street, New York, NY 10024; lepine@amnh.org.
[2] Département de Physique, Université de Montréal, C.P. 6128, Succursale Centre-Ville, Montréal, QC H3C 3J7, Canada; and Observatoire du Mont Mégantic; moffat@astro.umontreal.ca, sergey@astro.umontreal.ca, stlouis@astro.umontreal.ca.
[3] Visiting Astronomer, Canada-France-Hawaii Telescope.
[4] Killam Fellow of the Canada Council for the Arts.
[5] Department of Physics and Astronomy, University College London, Gower Street, London, WC1E 6BT, UK; pac@star.ucl.ac.uk, ljs@star.ucl.ac.uk, ajw@star.ucl.ac.uk.
[6] Visiting Astronomer, William Herschel Telescope.
[7] Moscow State University, Strongbox State Astronomical Institute, Universitetskij Prospect 13, 119899, Moscow, Russia; igor@sai.msu.ru.
[8] Instituto de Astronomía, Apartado Postal 877, C.P. 22860, Ensenada, México; gag@bufadora.astrosen.unam.mx.

have shown that radio continuum estimates of $\dot{M}$ must be revised downward by a factor ≈ 3 when one includes clumping effects. The downward revision of the estimated $\dot{M}$ values brings the new values in better agreement with estimates of $\dot{M}$ using clumping-independent empirical methods (St-Louis et al. 1988), which were originally thought to be in disagreement with commonly adopted values.

Models of WR spectra are now being developed to include the effects of wind clumping. These models treat clumping as a general behavior (through a filling factor f) and are not concerned with the detailed geometry of the clumps. Hence, Morris et al. (2000) have derived clumping filling factors of $f \sim 0.1$ from the spectrum of the WN8 star WR 147, using spectroscopic ratios between the line emission and the intensity of electron scattering wings. As it turns out, none of spectral analysis, radio and infrared continuum, or X-ray measurements can provide any substantial information about the actual clumping geometry. For example, compressed shells can yield the same result as discrete clouds (blobs).

Fortunately, the outflow velocities of WR winds are typically large enough that it becomes possible to Doppler-resolve spectroscopically different parts of the wind where material flows at different angles to the line of sight. This is especially obvious in the broad emission lines characteristic of WR spectra. The broad optical emission lines of all WR stars are found to be systematically variable on timescales of hours (Lépine, Moffat, & Henriksen 1996). These stochastic line profile variations (LPVs) show up as narrow ($\sigma_v \approx 100$ km s^{-1}) emission subpeaks moving on the tops of the emission lines. This strongly favors clumping as discrete elements (blobs) over concentric shells, which cannot produce the observed patterns (see also Lamers 1994).

The stochastic LPVs are to be distinguished from the periodic LPV patterns found in the lines of WR stars with close, massive OB companions (e.g., Moffat et al. 1998). In such binaries, the variability is thought to arise from the motion of an extra line-emitting volume located between the stellar components and believed to be associated with the collision shock zone between the winds of the WR star and its hot, massive companion (Brandi, Ferrer, & Sahade 1989; Luehrs 1997).

The stochastic LPVs must also be distinguished from the peculiar recurrent LPV patterns found in a small number of peculiar WR stars such as WR 6 and WR 134 (Morel et al. 1998, 1999). Although similar to clumplike stochastic LPVs at first glance, these recurrent LPV patterns are usually more intense (5%–10% of the line intensity) and consist of variable emission subpeaks that are relatively broader ($\sigma_v \approx 400$ km s^{-1}). The patterns of subpeaks are typically found to recur within a few days, and this phase-dependent variability pattern is also found to be epoch dependent. It is hypothesized that this recurrent variability is induced by the rotation of an azimuthally structured wind, which could result either from intense wind perturbations propagating from the surface of the star or from the existence of a compact companion orbiting close to the WR component.

Whereas periodic and recurrent LPVs are found only in some WR stars, stochastic LPVs have been found in all WR stars (and even one strong emission-line O star: Eversberg, Lépine, & Moffat 1998) monitored so far using high S/N, high-resolution, optical spectroscopy. Stochastic LPVs always consist of relatively narrow subpeaks, and no recurrent pattern has been observed to date. These are suspected to result from self-induced clumping in the wind, as a result of instabilities in the wind-driving mechanism (Gayley & Owocki 1995).

Lépine & Moffat (1999, hereafter Paper II) have recently developed a simple phenomenological model to reproduce the stochastic LPVs in WR emission lines. A similar "cloud model" has also been investigated by Kostenko & Kholtigin (1999). These models assume the wind to be made up of a large number of discrete elements in radial expansion (with over 10^4 elements per hour crossing the surface of a sphere centered on the star). Paper II also introduced a number of numerical methods for the analysis of spectroscopic time series of variable emission lines, which can be used to provide constraints on the geometry and dynamics of wind clumps. Modeling of the LPVs yields independent information about the wind velocity and acceleration rate, the size and range of the line emission volume, and some limited information about the inhomogeneous structure of the wind. The accuracy of LPV modeling depends on the statistics of the variability, and can be significantly improved by increasing the number of spectra in the time series.

In this paper, we present the results of an intensive spectroscopic and photometric monitoring campaign of the WR star HD 192103 (= WR 135). This star was selected because it is suspected to be single, is relatively bright ($V = 8.5$), and has very intense optical emission lines, in particular C III λ5696 and C IV λ5808. The star is also a prototype for spectral analysis models (Koesterke & Hamann 1995). Section 2 presents data from an intensive photometric campaign from telescopes in Arizona, Mexico, and Crimea during 1992–1997. Section 3 presents and analyzes a time series of 197 spectra obtained from the William Herschel Telescope (WHT) and from the Canada-France-Hawaii Telescope (CFHT) in 1994 June, in overlap with two of the photometric data subsets. Section 4 describes a phenomenological model for the LPV in a WR wind with clumps: simulations are presented and compared to the observations. Section 5 discusses the combined results from the photometric and spectroscopic time series and provides an interpretation for the line profile variability. Section 6 summarizes the results and provides suggestions for future observations.

2. PHOTOMETRY OF HD 192103

In order to explore the behavior of the continuum light in HD 192103, we have compiled three sets of photometric observations performed between 1992 and 1997.

1. The first set consists of extensive photometry (≈ 300 measurements in each UBV Johnson filter) collected between 1992 September and 1997 July by one of the automated 25 cm telescopes (APT) in Arizona (see Young et al. 1991 for a general description). This uses a conventional mode of observation, i.e., the following sequence of 10 s integrations: check star (ch, UBV)–sky (s, UBV)–comparison star (c, UBV)–WR 135 (wr, UBV)–c–wr–c–wr–c–s–ch. HD 192934 (A1 V) and HD 192533 (A2), respectively, were used as the check and comparison stars.

2. The second set was obtained in 1994 June–July using the 0.84 m telescope of the San Pedro Mártir Observatory (México) equipped with a one-channel photometer and nar-

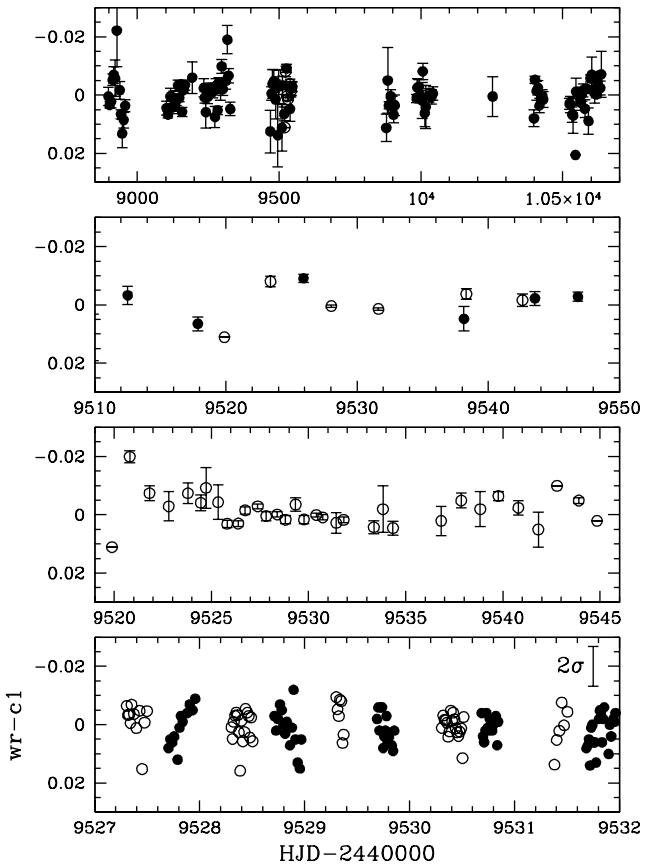

FIG. 1.—Photometric variability in the Wolf-Rayet star HD 192103. The upper section shows all available photometric data for HD 192103, in 5 day bins with 2 σ error bars. The second section from the top shows the APT data (*filled circles*) and the SPM + Crimea data (*open circles*), 5 day bins with 2 σ errors. The third section shows only the SPM + Crimea data, 0.5 day binned with 2 σ errors. Finally, the bottom section shows the original Crimea (*open circles*) and SPM (*filled circles*) data with a typical 2 σ error bar in the upper right-hand corner. All the panels show the difference (wr − c1) as a function of time between the WR star and a nonvariable comparison source.

rowband filter: $\lambda_0 = 5990$ Å, FWHM = 65 Å, covering a practically line-free region. We collected a total of 116 observations of $\sigma = 0.006$ mag accuracy each.

3. The third photometric set comprises data obtained in 1994 June at the 0.6 m telescope of the Crimean (Ukraine) Observational Station of GAISH with a one-channel photometer and two filters: the standard Johnson V band (91 observations, $\sigma = 0.008$ mag) and a narrowband filter identical to the SPM filter (91 observations, $\sigma = 0.012$ mag).

To bring the accuracy of the GAISH data more in line with the SPM observations, we blended the zero-point–adjusted narrowband and broadband data with relative respective weights 1:2, thus providing $\sigma = 0.007$ mag accuracy for the combined set. During the SPM and GAISH observations we used two stars in the vicinity of WR 135 as the check and comparison stars. To facilitate detectability of any long-term (weeks) or medium-term (days) trends in the flux variations, we adjusted the zero points in all available APT, SPM, and GAISH observations, binned the zero-point–shifted data to 5 or 0.5 day bins, and applied a 10% upper and 10% lower rejection rate to the data within each bin. The complete time series of photometric observations is presented in Figure 1.

From these observations, we conclude that the star is relatively quiet: variability is no more than ± 0.02 mag peak-to-peak on a timescale of 10–1000 days. Microvariability of order ± 0.01 mag on a 1–2 week timescale is clearly seen in the second section from the top. Note the excellent agreement between the APT and SPM + Crimea subsets. In particular, the star was relatively quiet during the time when the spectroscopic data were obtained (HJD 2,449,528.8–HJD 2,449,531.2), with night-to-night variability not exceeding ~ 0.005 mag.

A search for periodic patterns was made, with negative results. This rules out any modulation due to stellar rotation or the presence of a companion. The overall stability of the photometric time series is consistent with the star being either single or double with a very large separation. Any variable behavior observed in the emission lines should thus be ascribed to processes intrinsic to the wind of the WR star.

The wind of HD 192103 appears to be globally very stable on timescales of days to years. This is to be contrasted with the variable behavior of the wind emission lines, which suggest that the wind is unstable on small scales. The continuum basically arises in the wind, within a concentric shell at some distance from the stellar surface. While this geometry obviously makes the continuum flux sensitive to the presence of an expanding dense shell, it is much less sensitive to the propagation of a large number of discrete clumps. We will see below that clumping is more readily observed in the broad emission lines, which do provide a limited resolution of discrete overdensity features in the wind.

3. SPECTROSCOPY OF HD 192103

3.1. *Observations*

The spectroscopic data were obtained during a double-site monitoring campaign of WR 135. High-resolution spectra were collected at the 3.6 m Canada-France-Hawaii Telescope (CFHT) and the 4 m William Herschel Telescope (WHT).

At the WHT, the Utrecht Echelle Spectrograph (UES) was used at the Nasmyth focus with the TEK 1024 × 1024 CCD detector. Comparison stars BD +33°2642 (B2 IVp), BD +28°4211 (Op), and HR 7734 (A0 V) were used for the flux calibration and atmospheric correction. Standard reduction was carried out with IRAF. The resulting WHT time series consists of 107 spectra with a 3 pixel resolution $\simeq 0.165$ Å, and a signal-to-noise ratio in the continuum ≈ 350 per resolution element.

Unfortunately, at the CFHT part of the first night and the whole second night were lost due to bad weather. When the sky was clear, observations of WR 135 at CFHT were made with the f/8.2 spectrograph at the coudé focus with the RETICON detector. Standard reduction was carried out with IRAF. The resulting CFHT spectroscopic time series consists in 90 spectra with a 3 pixel resolution $\simeq 0.295$ Å, and a signal-to-noise ratio in the continuum ≈ 425 per resolution element.

The WHT and CFHT spectra were transformed by interpolation to a common wavelength grid, with fluxes normalized to unity relative to a pseudocontinuum level defined as the low-intensity region between the bright C III $\lambda 5696$ and C IV $\lambda 5804$ emission lines. (Because of emission-line contamination, the true continuum level cannot be objectively

defined in that part of the spectral regime.) The resulting data set is a uniform time series consisting of 197 spectra with a 3 pixel resolution $\simeq 0.3$ Å, and a signal-to-noise ratio in the continuum ≈ 450 per resolution element. The time series covers a 65 hr interval, but with a number of gaps of several hours. This large, unique data sample yields a high statistical significance to the results.

The resulting combined spectroscopic time series is presented in Figure 2. Only three orders from the WHT échelle spectra are shown here; these match the full spectral regime observed at CFHT. The complete data set from WHT will be presented and analyzed elsewhere (Lépine et al. 2000). To emphasize the variable features in the emission lines, Figure 2 plots only the instantaneous deviation of individual spectra from the mean spectrum as a function of time. This time series of residuals clearly shows the existence of variability patterns in the C III λ5696 line and in the C IV λ5808 doublet. The LPV pattern appears to consist of a number of transient, narrow peaks and troughs that gradually move toward the nearest emission-line edge, where they disappear.

We measure the magnitude of the line variability by calculating the mean standard deviation σ as a function of wavelength over the $N = 197$ spectra in the time series

$$[\sigma(\lambda)]^2 = (N-1)^{-1} \sum_{i=1}^{N} \left[S_i(\lambda) - N^{-1} \sum_{i=1}^{N} S_i(\lambda) \right]^2 , \quad (1)$$

where $S_i(\lambda)$ represents the ith spectrum in the time series. The mean standard deviation is plotted in Figure 2. Note that the variability across the top of the C III λ5696 emission line is ≈ 25 times larger than the variability in the continuum regions. This leaves no doubt that this emission line is intrinsically variable.

3.2. *Variability Patterns*

The line profile variability in C III λ5696 is dominated by narrow, transient, emission features (subpeaks) that tend to

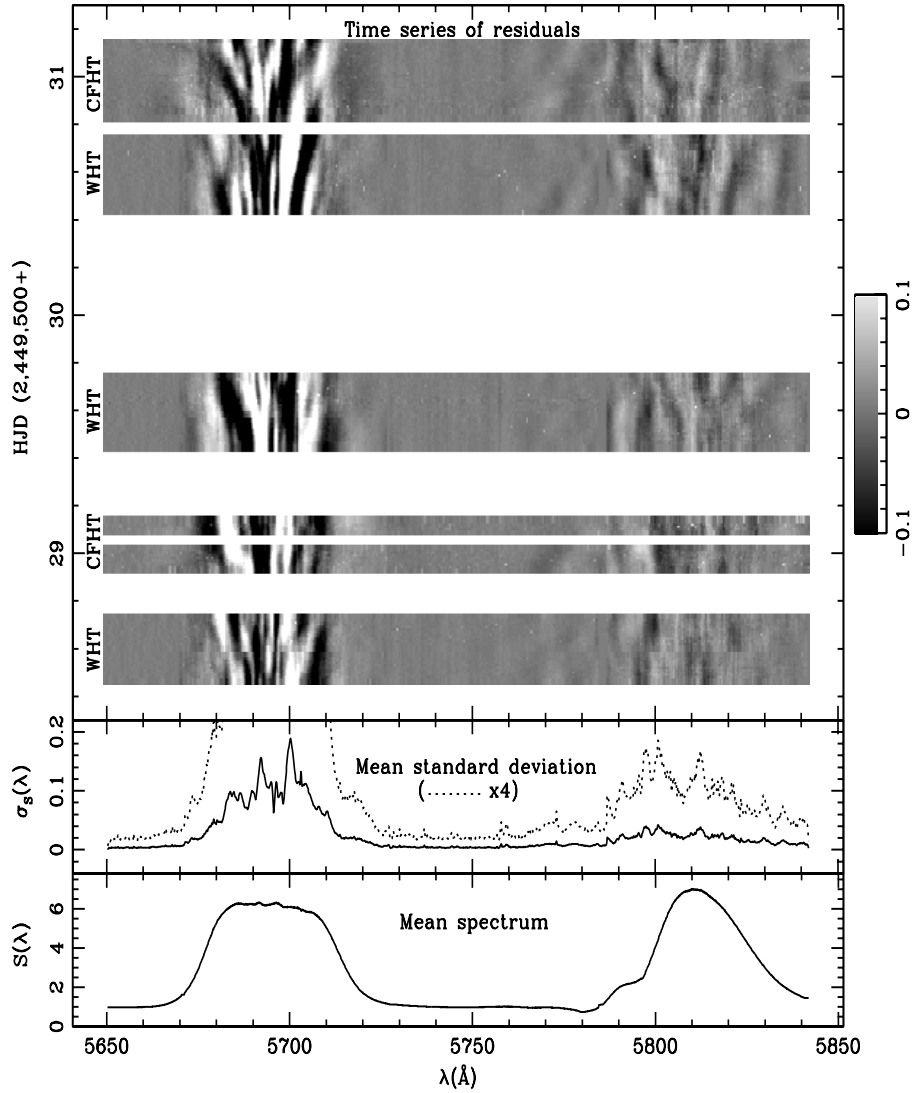

FIG. 2.—Combined CFHT and WHT spectroscopic monitoring of HD 192103. The mean profile for the whole data set is shown, along with the mean standard deviation, which indicates 4 times as much variability in the C III λ5696 emission line as in the C IV λ5808 doublet region. The gray-scale part is a time series of the residuals (obtained after subtracting off the global mean profile), detailing the variability pattern as a function of time. Note how the narrow emission features (*subpeaks*) appear to systematically move away from the line center. This pattern is consistent with the C III and C IV emission arising in a volume where the wind is clumped and accelerating away from the star.

move toward the nearest line edge. A subpeak event consists of the stochastic appearance and subsequent disappearance after a given time of a transient emission feature. The pattern of peaks and troughs in the residual spectra appears to be completely degraded after a number of hours. Two effects actually participate in the degradation of the subpeak pattern: (1) the finite duration of a subpeak event and (2) the motion of the subpeak across the spectrum. To disentangle and quantify both effects, we have devised a numerical tool which we call the degradation function (see Paper II).

The degradation function, denoted $\sigma_D(a, \Delta t)$, basically measures the mean standard deviation between spectra separated by an interval Δt. However, $\sigma_D(a, \Delta t)$ also accounts for the possible motion away from line center of the subpeak features, by including the parameter a. If the spectroscopic time series was a continuous function in $S(\xi, t)$ [where $\xi = (\lambda - 5696)c/5696$ is the line-of-sight Doppler velocity calculated for the λ5696 transition with c the speed of light] in the time interval $[t_1, t_2]$ the degradation function would be mathematically expressed as

$$[\sigma_D(a, \Delta t)]^2 = \int_{t_1}^{t_2} dt \int_{-v}^{v} d\xi [S(\xi, t) - S(\xi - a\Delta t v^{-1}\xi, t - \Delta t)]^2 , \quad (2)$$

where it is assumed that the line profile spans the interval $-v < \xi < v$ in line-of-sight velocity space. Figure 3 illustrates how the degradation function works. Two spectral elements (*bold segments*) separated by an interval Δt are compared. The former segment is stretched before it is compared to the latter segment, so as to simulate the pattern in line-of-sight velocity space (ξ) resulting from the accelerated expansion of a wind at a constant rate (a) up to a velocity (v).

Figure 4 shows the analysis of variability patterns in the C III λ5696 emission line. Results show that subpeak events are consistent with clumps in radial acceleration at a mean rate $a \approx 50$ km s^{-1} hr^{-1}, in which case the typical duration of subpeak events is found to be $\Delta t \approx 7.5$ hr. Assuming the duration of an event to be indicative of the time it takes for a wind clump to move across a thick shell of C III λ5696 emission centered on the star, then the velocity range spanned by the shell is $\Delta v = a\Delta t \approx 375$ km s^{-1}. In other words, upon ceasing to emit in C III λ5696, the radial velocity (relative to the star) of a wind clump is $\approx$375 km s^{-1} larger then when it started to emit.

3.3. *Size and Shape of the Variable Subpeaks*

Previous analyses (e.g., Paper II; Lepine, Eversberg, & Moffat 1999, hereafter Paper III) of LPVs in nine WR stars, including WR 135, indicated that the variable subpeaks tend to be narrower near the line center ($\sigma_\xi \approx 50$ km s^{-1}) than near the edges ($\sigma_\xi \gtrsim 150$ km s^{-1}). The present new, superior data set allows us to verify this once more to a greater level of precision in the case of WR 135. We use the wavelet spectrum method, described and discussed in Paper II and Paper III, to quantify the mean line-of-sight velocity dispersion σ_ξ associated with the variable subpeaks.

Figure 5 shows a contour plot of the mean (time-averaged) wavelet power spectrum $\langle \tilde{R}(\xi, \sigma_\xi) \rangle$ of the time series of the residuals $R(\xi, t)$ (see Paper III for a complete description of the wavelet power spectrum), again using $\xi = (\lambda - 5696)c/5696$. The morphology of the power distribution in the $[\xi, \sigma_\xi]$ plane confirms that transient emission subpeaks are narrower near the center of the line

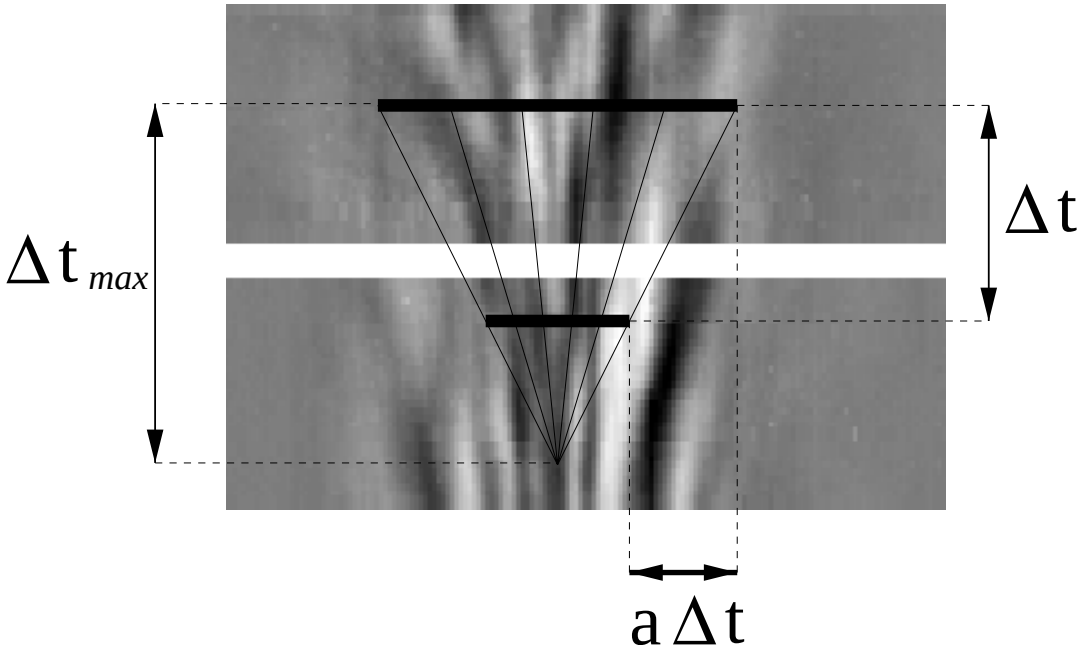

FIG. 3.—Schematic illustration of the degradation function, used to analyze the variability patterns superposed on the C III λ5696 data in the upper part of Fig. 2. Points in the upper segment are compared to matching points in the lower segment (*bold lines*). The mean standard deviation is computed for all such segments in the data separated by an interval $\approx \Delta t$. Note that when a given value of the dilation factor a is used, no output is generated in the degradation function for values of $\Delta t > \Delta t_{max}$. A minimum value of the rms standard deviation between the segments is expected for a value of a that matches the radial acceleration of clumps in the wind.

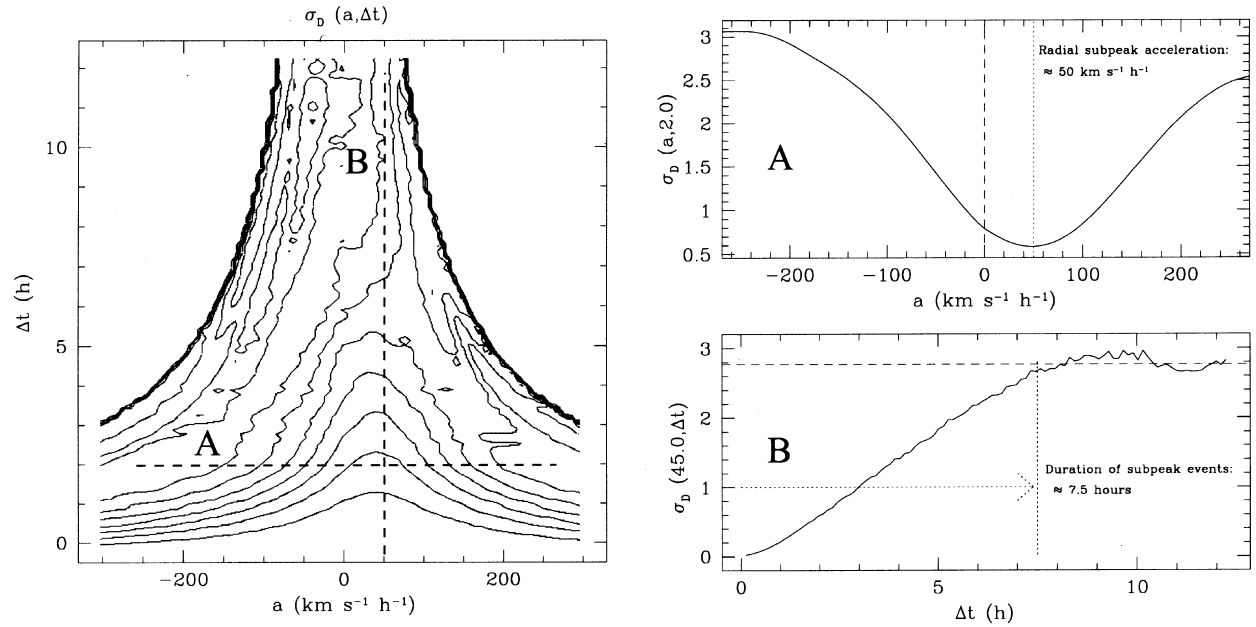

FIG. 4.—Degradation function $\sigma_D(a, \Delta t)$ of the subpeak pattern in the C III λ5696 emission line. *Left*: Contour plot of $\sigma_D(a, \Delta t)$. Dashed lines denote the regions plotted on the right. *Upper right*: σ_D as a function of the acceleration a along $\Delta t = 2.0$ hr. The minimum denotes the acceleration that one must use in order to follow the motion of the subpeaks on the line. Conversely, this provides an estimate of the mean radial acceleration of the clumps in the wind. *Lower right*: σ_D as function of the time interval Δt for a follow-up acceleration $a = 50$ km s^{-1} hr^{-1}. The standard deviation monotonically increases as the signal is degraded until it reaches a plateau phase, indicating that the subpeak pattern has been completely recycled. The time to reach the plateau phase is an estimate of the minimal timescale of subpeak events in the C III λ5696 emission line.

($\xi = 0$) than near the edges. This suggests an anisotropic velocity dispersion within the wind clumps (see Paper II).

Near the line edge ($700 < |\xi| < 1050$ km s^{-1}), we find the wavelet power distribution to be shifted in scale relative to the power distribution near the line center ($|\xi| < 350$ km s^{-1}). More precisely, the power distribution for variable features at large $|\xi|$ indicates a deficiency on the small-scale range as compared to the power distribution of vari-

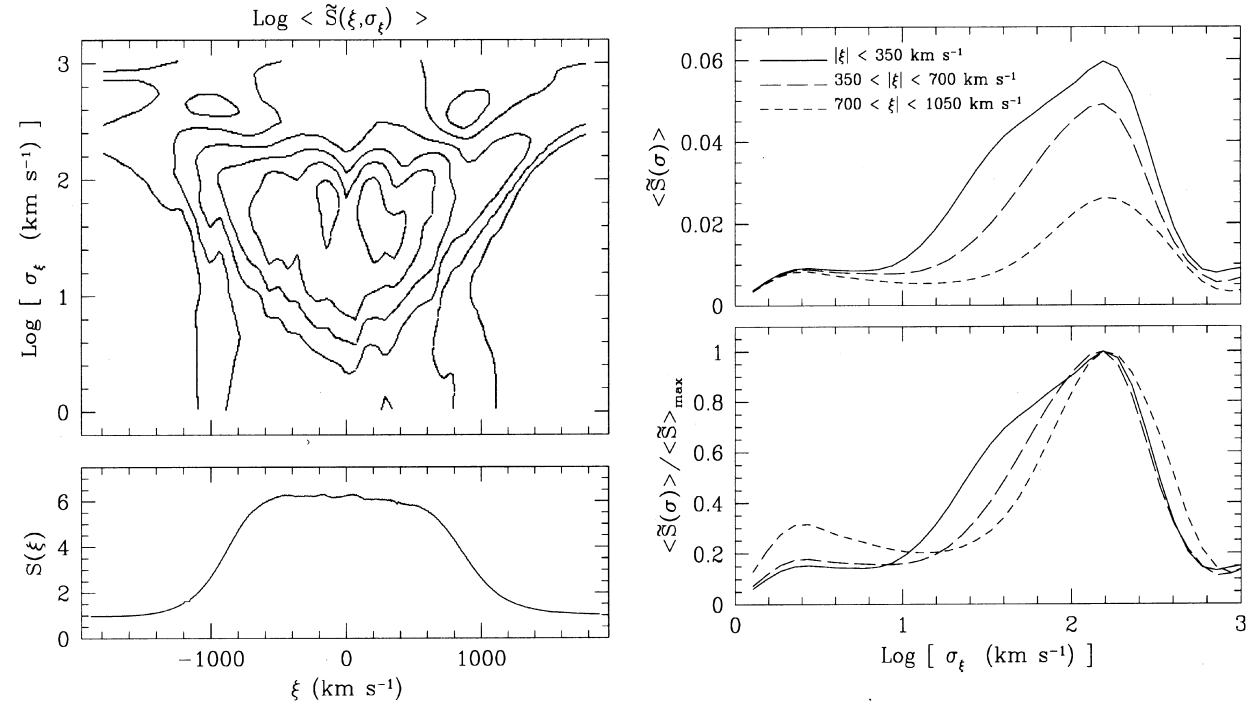

FIG. 5.—*Left*: Contour plot of the mean wavelet power spectrum $\langle \tilde{S}(\xi, \sigma_\xi) \rangle$ for the C III λ5696 emission line. *Top right*: Mean distribution of $\langle \tilde{S}(\xi, \sigma_\xi) \rangle$ at different distances from the center of the line. Note that not only does the power decrease as one goes away from line center, but the power distribution is also shifted toward larger scales (see normalized plot at bottom right). As was shown in Paper II, this loss in small-scale variability corresponds to a smoothing out of the variability pattern resulting from a larger projected velocity dispersion. This particular distribution is consistent with subpeaks having a *mean* velocity dispersion $\sigma_\xi \simeq 60$ km s^{-1} near the line center ($|\xi| < 350$ km s^{-1}) and $\sigma_\xi \approx 150$ km s^{-1} near the edges ($700 < |\xi| < 1050$ km s^{-1}).

able features at small $|\xi|$ (see the lower right-hand panel in Fig. 5). There is a measurable shift in the small-scale part of the wavelet power distribution of ≈ 0.4 in $\log(\sigma_\xi)$, which indicates that the narrowest variable features at large $|\xi|$ tend to be ≈ 2.5 times broader than those near $|\xi| = 0$ (see Paper II).

The power distribution for variable features in the range $700 < |\xi| < 1050$ km s^{-1} is consistent with a mean variable subpeak width $\sigma_\xi \simeq 150$ km s^{-1} in that range [from the maximum at $\log(\sigma_\xi) = 2.2$; see Paper III]. It thus follows that variable features near the line center ($|\xi| < 350$ km s^{-1}) have a mean width $\sigma_\xi \simeq 60$ km s^{-1}. We can model the typical width of subpeak features at a given location on the line profile with (see Paper II)

$$\sigma_\xi(\xi) = \sqrt{\frac{\xi^2}{v_{\rm line}^2}(\sigma_{v_r})^2 + \left(1 - \frac{\xi^2}{v_{\rm line}^2}\right)(\sigma_{v_\theta})^2}\ , \qquad (3)$$

where $v_{\rm line} \approx 900$ km s^{-1} is the mean velocity of the C III emission range (i.e., approximately half the width of the C III λ5696 emission line). The parameter σ_{v_r} is the velocity dispersion of the clumps in the direction of propagation (i.e., away from the star), while σ_{v_θ} is the velocity dispersion perpendicular to that direction. From the mean values of σ_ξ measured in the ranges $|\xi| < 350$ km s^{-1} and $700 < |\xi| < 1050$ km s^{-1}, we can use equation (3) to derive matching values of σ_{v_r} and σ_{v_θ}. Our measured mean values of σ_ξ (i.e., 60 and 150 km s^{-1}) yield $\sigma_{v_r} \simeq 175$ km s^{-1} and $\sigma_{v_\theta} \simeq 50$ km s^{-1}. As was discussed in Paper II, the fact that $\sigma_{v_r} \approx 3.5\sigma_{v_\theta}$ indicates that wind inhomogeneities have a significantly larger velocity dispersion in their direction of propagation through the wind, which is consistent with the clumps being associated with strong shocks in the direction of wind acceleration.

A quantification of the anisotropy in the velocity dispersion of the clumps is crucial for the analysis of the line profile shape. The "roundness" of an optically thin emission line basically depends on the velocity range over which the line emission occurs. This in turns depends on (1) the magnitude of the wind acceleration in the volume where line emission occurs, and (2) the magnitude of the "turbulent velocity" within this volume. If this "turbulent velocity" happens to be larger in the radial than in the transverse direction, then line broadening will be increased near the line edges. But in effect, it is only near the edges that line broadening effects can be measured, especially in broad, flat-top profiles such as C III λ5696. Assuming that the width of the variable subpeaks is a measure of the local "turbulent velocity" in the wind, then one needs to use the widths of the subpeaks that are near the edge (i.e., use σ_{v_r}) to compare with the "turbulent velocity" as inferred from the roundness of the line profile (see § 4.3).

3.4. *Variability Levels*

The significantly low contribution of the instrumental noise $\sigma_{\rm inst}$ from the observed variability $\sigma(\lambda)$ in the C III λ5696 region allows one to study in detail the intensity of the intrinsic variability across the emission line profile. We estimate $\sigma_{\rm intr}$, the intrinsic variability, by subtracting an estimated contribution from the instrumental noise $\sigma_{\rm inst}$. Using the variability in the (relatively line-free) continuum region $\lambda\lambda$5730–5770 as a reference for the instrumental noise; we estimate $\sigma_{\rm cont} = 0.0037$ continuum units. Assuming that most of the instrumental noise is due to count statistics, the instrumental noise across the C III λ5696 emission line can thus be approximated by

$$\sigma_{\rm inst}(\lambda) = 0.0037\sqrt{S(\lambda)}\ . \qquad (4)$$

We then calculate $\sigma_{\rm intr}$ using

$$\sigma_{\rm intr}(\lambda)^2 = \sigma(\lambda)^2 - \sigma_{\rm inst}(\lambda)^2\ . \qquad (5)$$

A plot of $\sigma_{\rm intr}(\xi)$, for the C III λ5696 emission lines, with $\xi = (\lambda - 5696)c/5696$, shows that the intrinsic line variability is significantly smaller for large values of $|\xi|$, i.e., near the edges of the line (see Fig. 6). Near the line center the variability is $\approx 2\%$ of the line intensity, whereas it is only $\approx 1\%$ near the edges. This behavior is in slight disagreement with previous claims that the variability across WR emission-line profiles is directly proportional to the local line intensity (with neglect of the P Cygni absorption edges; e.g., Moffat & Robert 1991).

Part of this effect is due to the fact that emission subpeaks near the edge of the line tend to be broader. We have shown in Paper II that this has the effect of reducing the apparent variability. At a given point on the line profile, the variability is expected to be proportional to the inverse square root of the width of subpeak features at that point.

We account for the subpeak width effects by using equation (3) and applying a model of the observed variability levels, where the number density of subpeaks is constant across the line profile, i.e., at any point on the line profile,

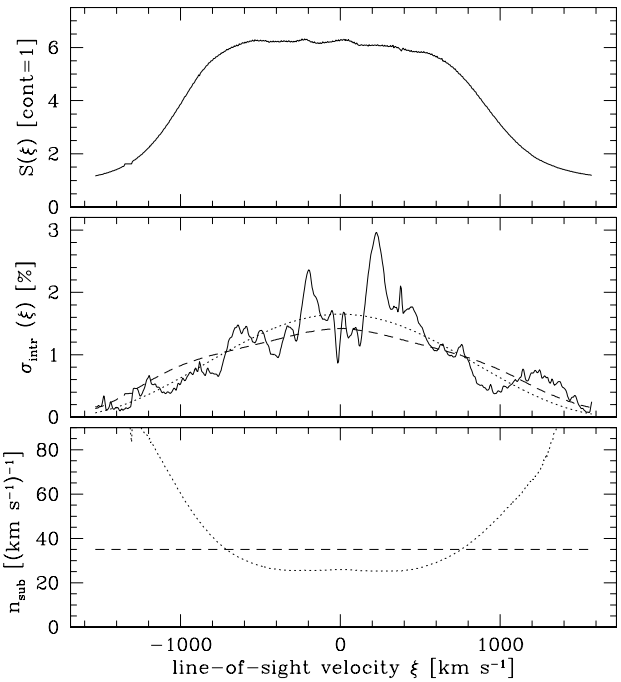

FIG. 6.—*Top*: Mean C III λ5696 emission-line profile for HD 192103 from our spectroscopic time series. The profile is plotted in line-of-sight velocity space ξ. *Middle*: Intrinsic variability across the line profile. Variability levels reach 2% of the line emission near the center of the line and fall below 1% of the line emission near the edges. *Bottom*: Estimate of the local density of subpeaks (in subpeaks per km s^{-1}), if we assume that the whole emission line is made up of discrete emission subpeaks. The dashed line shows a model in which the number density of subpeaks is constant across the line. The dotted line, which provides a marginally better fit to the line variability, is a model in which the number density increases near the line edge (see § 3.4).

the emission arises from a constant distribution of clumps in line-of-sight velocity space. The bottom panel in Figure 6 represents the density of clumps in line-of-sight velocity space for this model (*dashed line*), while the corresponding variability levels are overplotted with the observed variability profile in the middle panel. For a model with constant density of clumps in ξ, the best fit is obtained for a density of 35 clumps per km s^{-1}, which means that the whole emission line (which is $\approx$2000 km s^{-1} broad) arises from a total of $\sim 7 \times 10^4$ clumps.

While this model matches with the observed variability levels reasonably well, we found that an alternate model provides a marginally better fit to the observations. In this alternate model, the number density of clumps increases for large values of $|\xi|$. One interpretation of this model is that the C III emission occurs within a certain range of wind velocities over which the number of clumps is not uniform. Specifically, clumps tend to pile up at large wind velocities, which naturally occurs if the acceleration rate decreases with increasing velocity (i.e., the acceleration rate decreases with distance from the star). This results in a larger number of clumps having large values of $|\xi|$. This effect is discussed further in § 5.

3.5. *Variability Correlations between* C III λ5696 *and* C IV λ5808

We compare the variability patterns found in different emission lines by using a cross-correlation technique (see Lépine 1996). We define the cross-correlation function $C(\lambda_0, \Delta\lambda)_i$ for the ith spectrum in the time series as

$$C_{[\lambda_0,\Delta\lambda]}(\lambda)_i = \int_{\lambda_1}^{\lambda_2} w(x + \lambda, \Delta\lambda) S_i(x + \lambda_0 - \lambda) S_i(x) dx \ . \quad (6)$$

The function $w(x + \lambda, \Delta\lambda)$ is the window and is a mathematical expression of the form:

$$w(x, \Delta x) = 1, \text{ for } |x| < \Delta x \ ; \quad (7)$$
$$= 0, \text{ for } |x| > \Delta x \ .$$

The use of a window allows one to select a particular segment of length $\Delta\lambda$, centered on λ_0, which is then cross-correlated along the full length of the signal. If the segment exactly repeats itself at any point in the signal, then the correlation at that point is expected to be $C_{[\lambda_0,\Delta\lambda]}(\lambda) = 1.0$.

To increase the statistical significance, we combine the information in all of the spectra in the time series. The combined, average cross-correlation function $\overline{C}_{\lambda_0,\Delta\lambda}(\lambda)$ for the N spectra in the time series is simply

$$\overline{C}_{[\lambda_0,\Delta\lambda]}(\lambda) = (N-1)^{-1} \sum_{i=1}^{N} C_{[\lambda_0,\Delta\lambda]}(\lambda)_i \ . \quad (8)$$

A more rigorous cross-correlation method would normally require one to perform the correlation in $\Lambda = \log(\lambda)$ space because Doppler shifts are given by $\Delta\lambda = \lambda_0 \xi c^{-1}$, with ξ the line-of-sight velocity of the emitting material, and c the speed of light. In λ space, the shifts are proportional to λ_0, the rest wavelength of the emission line, and thus vary across the spectrum, while in Λ space, the Doppler shifts are given by $\Delta\Lambda = \log(1 + \xi)$ and are independent of λ_0. In our case, however, the C III and C IV emission features are very close in λ space, and the ratio in the Doppler shifts in these lines is $\lambda_{5696}/\lambda_{5812} = 0.98$, i.e., close to unity. This small difference in the $\Delta\lambda$ in the two lines will attenuate the correlation between the variability patterns, but the effect will be negligible.

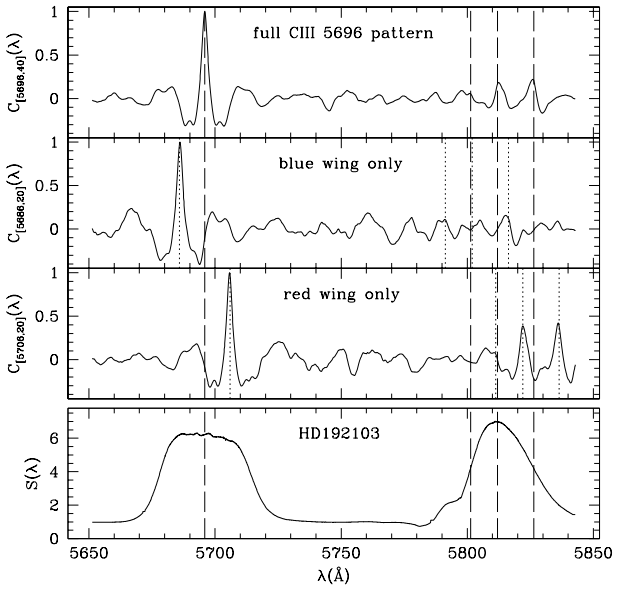

FIG. 7.—Cross-correlation function of the variability pattern in the C III λ5696 emission line. Results are shown for the full pattern (5676–5716 Å), the blue side (5676–5696 Å), and the red side (5696–5716 Å). Dashed lines show the location of the C III $\lambda\lambda$5696, 5826 and C IV $\lambda\lambda$5801, 5812 transitions, while dotted lines indicate the expected location of correlation peaks. No significant correlation is found with the blue sides because of contamination by the variable P Cygni absorption troughs in C IV line. A significant correlation is found between the red side of the C III λ5696 line and the red side of C IV λ5812, the C IV doublet member least affected by the blended P Cygni variability. A correlation peak matches the expected location of the blended C IIIλ5826 emission line, suggesting that this line varies as C IIIλ5696.

The cross-correlation using the full C III λ5696 pattern as a response is show in Figure 7 (*top panel*). The cross-correlation yields only a marginally significant response with the C IV λ5808 doublet for the λ5812 component. We know that the LPVs in C IV λ5808 do not arise only in emission, as in C III λ5696, but also in P Cygni absorption components.

Fortunately, the P Cygni components should affect only the blue side of the emission profile. Keeping this in mind, we performed the cross-correlation analysis using only the LPV patterns on the blue or on the red wings of C III λ5696 (see Fig. 7). The results are conclusive: no correlation is found with the blue wing, but a significant correlation response is found at the expected positions of the red wing of C IV λ5812 (the red wing of C IV λ5801 is confused with the P Cygni blue edge of C IV λ5812).

Unexpectedly, we also obtained a significant response near λ5838, about a dozen angstroms redward of the C IV λ5812 response. Upon checking the Kurucz line tables[9] (Smith et al. 1995), we found that this wavelength matches with the expected location of the red wing of the C III λ5826 emission line. Hence, the C IV λ5808 emission feature appears to be a triplet, comprising the relatively intense C IV

[9] http://cfa-www.harvard.edu/amdata/ampdata/kurucz23/sekur.html.

λ5801 and C IV λ5812 lines, and the weaker C III λ5826 line. Both C IV components are suspected to have the same strength, since the associated P Cygni absorption features appear to be similar in strength. The C III component, however, is definitely weaker, since we do not distinguish any strong emission component at that location in the mean profile. We believe that the fact that we can detect the variability from C III λ5826 among the C IV complex variability suggests that the relative variability in this C III line is probably stronger than in C IV, just as we observe for C III λ5696. The blue edge of C III λ5826 however, is probably confused with the variability in the C IV lines, which explains why we find a stronger correlation when using only the red edge of C III λ5696.

4. EMISSION-LINE VARIABILITY MODEL FOR A CLUMPED WIND

4.1. *The Wind Velocity Law*

We proceed to try and reproduce the observed LPVs by modeling line emission from a clumped, radially accelerated wind. We use the general phenomenological model described in Paper II to reproduce the line profile variability in the C III λ5696 emission line. This model assumes the wind to be made up of a large number of independent mass elements called discrete wind emission elements or DWEEs. We do not make any specific assumption about the shape and structure of these DWEEs, apart from assuming that their volume is significantly smaller than the characteristic scale of the wind (R_*). Hence they may occur in any arbitrarily large number, and their angular size as seen from the star is assumed to be negligible, i.e., they are treated as point sources.

The kinematics of the DWEEs are assumed to follow on average a radially outward directed wind velocity law $v = v(r)$. In this paper, we adopt a WR wind velocity law similar to that introduced by Hillier & Miller (1999), which is a linear superposition of two so-called β-laws:

$$v(r) = V_0 + (V_\infty - V_{\rm ext} - V_0)(1 - R_*/r)^{\beta 1} + V_{\rm ext}(1 - R_*/r)^{\beta 2} . \quad (9)$$

In equation (9), V_0 is the initial wind velocity at the stellar core ($r = R_*$), and V_∞ is the wind terminal velocity (at $r \to \infty$). Parameter $V_{\rm ext}$ and exponents $\beta 1$ and $\beta 2$ govern the acceleration rate in the wind. In a β-law, when the β exponent is close to 1.0, most of the acceleration occurs within a short range from the stellar core. Larger values of the β exponent, on the other hand, yield a lower local acceleration rate, which occurs over a larger distance range. By using a combination of two β-laws, one allows for a combination of short-range and long-range wind acceleration, as suggested in theoretical works of WR winds (Springmann 1994; Gayley, Owocki, & Cranmer 1995; Hillier & Miller 1999). Based on previous investigations (see Paper II), we set $\beta 1 = 1$, which is the value of the exponent that has traditionally been used in WR wind models, and adopt $\beta 2 = 10$ (e.g., Moffat 1996) to provide for an extra wind acceleration at large distances from the core.

The relative importance of the $\beta 2$ term compared to the $\beta 1$ term is governed by the parameter $V_{\rm ext}$. For $\beta 1 = 1$ and $\beta 2 = 10$, a small value of $V_{\rm ext}$ (e.g., $V_{\rm ext} < V_\infty/2$) implies that most of the acceleration occurs near the core, whereas a larger value of $V_{\rm ext}$ (e.g., $V_{\rm ext} > V_\infty/2$) means that long-range acceleration effects predominate. Reliable estimates of the terminal wind velocity for HD 192103 are $V_\infty \simeq 1405$ km s^{-1}, from maximum displacement of the black absorption trough in UV lines (Prinja, Barlow, & Howarth 1990), and $V_\infty \simeq 1450$ km s^{-1}, after modeling of the 2.058 μm He I line emission feature (Eeenens & Williams 1994). We adopt $V_\infty = 1400$ km s^{-1}. We also adopt a typical value of $V_0 = 100$ km s^{-1}, as the initial wind velocity at the stellar core (e.g., Dessart et al. 2000).

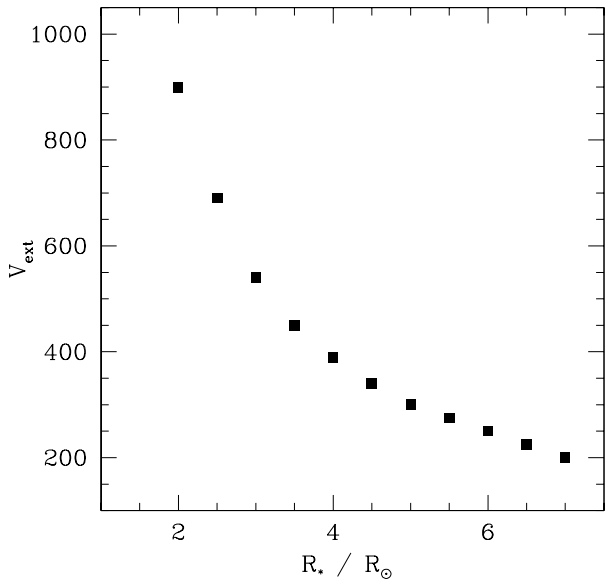

FIG. 8.—Values of the velocity law parameter $V_{\rm ext}$ required to match the acceleration rate measured in the C III λ5696 variable patterns, for different values of R_*. Large values of $V_{\rm ext}$ imply that the wind is still being accelerated at large distances from the star, whereas smaller values of $V_{\rm ext}$ imply that most of the acceleration occurs near the WR surface (see § 3). Current models favor small WR radii ($R_* \lesssim 3\ R_\odot$), which suggest that wind acceleration in HD 192103 occurs over a large distance range.

The only free parameters in equation (9) are R_*, the stellar core radius, and $V_{\rm ext}$, which controls the relative magnitudes of the long-range and short-range acceleration rates in the wind. We use our estimate of the acceleration rate in the C III λ5696 emission line to constrain the values of R_* and $V_{\rm ext}$; the results are shown in Figure 8. One sees that increasing values of $V_{\rm ext}$ must be used if one believes in smaller values of R_*.

In Figure 9, we compare the velocity laws required to fit the observed acceleration rate in the C III λ5696 line for two different values of the stellar core radius ($R_* = 2\ R_\odot$ and $7\ R_\odot$). For a larger radius, the velocity law does not deviate strongly from the traditional $\beta = 1$ velocity law, whereas a smaller radius requires a much larger deviation from the traditional β-law. Recent spectral analysis of WR emission lines (using a clumped wind model) yields a stellar core radius $R_* \approx 3.3\ R_\odot$ for WR 135 (Dessart et al. 2000); we adopt the same value for our velocity-law model. This then requires $V_{\rm ext} \approx 500$ km s^{-1} in order to fit the observed wind acceleration rate. We note that the adoption of a different value of R_* does not change the form of the velocity law, apart from a distance scale factor, as long as $V_{\rm ext}$ is accordingly adjusted to fit the observed wind acceleration rate (see Fig. 9). We are thus confident that the following results on the wind dynamics remain valid in general for a range in R_* of about 1–10 $R_\odot$, the only difference being in the physical scale of the wind.

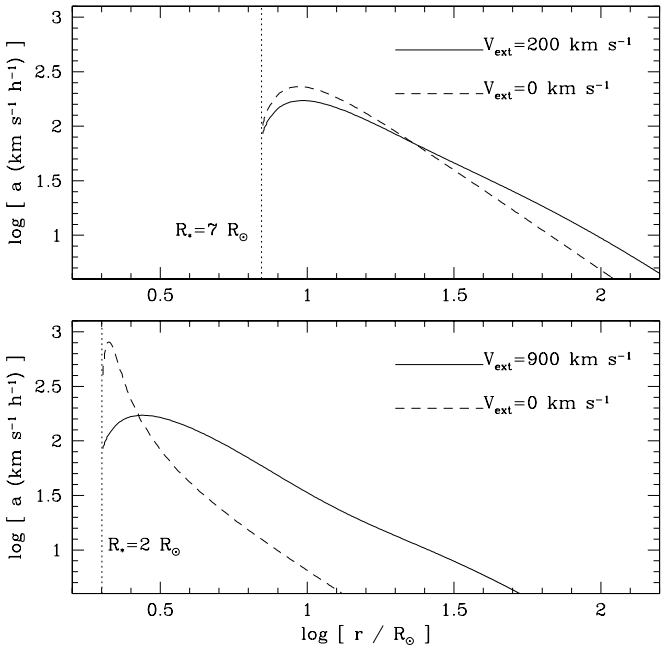

FIG. 9.—Wind acceleration as a function of distance for two different values of the hydrostatic stellar core ($R_* = 2\ R_\odot$, and $R_* = 7\ R_\odot$). The dashed lines show the acceleration for the traditionally used wind velocity law (with $\beta 1 = 1$ and no component in $\beta 2$, i.e., $V_{\rm ext} = 0$; see eq. [9]). The continuous line shows the acceleration for a wind velocity law that would match the observations best. Note that for the $R_* = 2\ R_\odot$ case, although the required acceleration rate at $r \approx 10\ R_\odot$ is significantly larger than for the $V_{\rm ext} = 0$ model, it is still smaller than for the same range in the $R_* = 7\ R_\odot$ model.

4.2. *Internal Clump Dynamics*

Time-dependent emission-line profiles are generated assuming the wind to be optically thin. The emission from individual DWEEs basically depends on their distance from the star. DWEEs also have associated velocity dispersions, which are different in the radial (σ_{v_r}) and azimuthal ($\sigma_{v\theta}$) directions. In our model, we reproduce this anisotropy with the formula

$$\sigma_\xi^2 = (\sigma_{v_r} \cos\theta)^2 + (\sigma_{v\theta} \sin\theta)^2 , \qquad (10)$$

which gives the line-of-sight velocity dispersion from a DWEE traveling along a trajectory radial to the star and making an angle θ with the line of sight. (This is actually another form of eq. [3].) Following the results from Paper II and the analysis of the current spectroscopic data on WR 135 (see § 3.3), we adopt $\sigma_{v_r} = 175$ km s^{-1} and $\sigma_{v\theta} = 50$ km s^{-1}.

4.3. *Ionization Structure and Line Emission*

Line emission from one DWEE will occur only if it lies at a distance from the star where the ionization equilibrium is consistent with emission from the required transition. WR winds have strong ionization stratification (Willis 1982; Rochowicz 1997; Herald et al. 2000), and the emission from different emission lines arises from a stratification of concentric shells centered on the star. The flat-top morphology of the C III λ5696 line indicates that it is formed within a relatively small range of radial velocities, which might at first suggest that the line is formed relatively far away, near where the wind reaches its terminal velocity, and where it has a low acceleration rate. However, because the width of C III λ5696 clearly indicates that the line is formed at a fraction of the terminal velocity ($\approx 0.7 v_\infty$), we know that the wind is still accelerating in these regions. The flat-top shape therefore suggests that most of the C III λ5696 line emission arises in a spatially relatively thin shell centered on the star.

The inverse problem of deriving the thickness of the emitting shell of material has been worked out by Ignace et al. (1998). It turns out that in the optically thin case, it is very easy to derive directly the thickness in radial velocity space of the line-emitting material from the shape of the line profile. The line emission as a function of radial (in the star's rest frame) wind expansion velocity $E = E(v_r)$ can be estimated as follows:

$$E(v_r) = -v_r \left[\frac{d}{d\xi} S(\xi) \right]_{\xi = v_r} , \qquad (11)$$

where $S = S(\xi)$ is the shape of the emission line in projected velocity space. The information necessary to derive $E(v_r)$ is contained mostly in the specific shape of the shoulders of the emission line. Both the blue ($\xi < 0$) and the red ($\xi > 0$) sides of the emission line can be independently used to estimate $E(v_r)$. In hot stars, the blue edge is sometimes altered by the presence of a P Cygni absorption edge, whereas the red edge can deviate from a pure, optically thin profile because of the presence of an electron scattering wing or, for lines formed close to the star, from occulting effects.

In our case, the C III λ5696 emission line has no obvious significant P Cygni component; therefore, its blue edge yields a more reliable estimate of $E(v_r)$. The velocity regime derived from the red edge is clearly broader (see Fig. 10), which suggests a contamination from the electron scattering

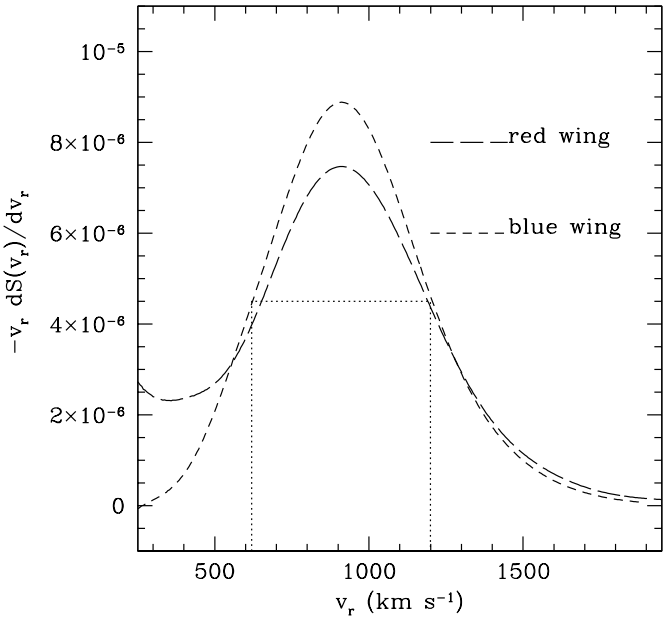

FIG. 10.—C III λ5696 line emissivity as a function of the bulk radial velocity of the wind v_r, estimated from the shape of the emission line. The result is shown for both the red and blue edges of the line. The red edge is altered by the electron scattering wing; the blue edge estimate is thus more reliable. This plot shows that maximum C III line emission occurs around the point where the wind has reached $v_r = 915$ km s$^{-1} = 0.65 v_\infty$.

wing, which tends to add an extra broadening to the red side of the line profile.

The emission is centered on the wind expansion velocity $v_r = 915$ km s^{-1} $= 0.65 v_\infty$, which we will adopt as the mean location in radial velocity space relative to the star of the C III emission-line region. Because the wind is still being accelerated in that velocity range, there is a monotonic relation between v_r and the actual distance r from the surface. Using our adopted velocity law, the location at which $v_r = 0.65 v_\infty$ is at $r \simeq 15\ R_*$ from the center of the star.

The range of the C III λ5696 line emission, in velocity space, extends from $\approx$630 km s^{-1} to $\approx$1200 km s^{-1} (see Fig. 10), where this emission range is defined as the full width at half-maximum of $E(v_r)$. Part of this $\approx$570 km s^{-1} dispersion of line emission in velocity space is due to the local, intrinsic velocity dispersion of the clumps in the wind, which was estimated to be $\approx$175 km s^{-1} in the radial direction (§ 3.3). If we subtract the square of the intrinsic velocity dispersion from the square of the apparent velocity range, we get the square of the actual range of the line emission in bulk wind velocity space. The actual range of emission is thus estimated to be $\approx$540 km s^{-1}, which means that C III emission occurs in the range $645 < v_r < 1185$ km s^{-1}, or $0.46 < v_r/v_\infty < 0.84$. This range is basically consistent with the emission range for C III λ5696 derived by spectral analysis of WR 135 spectra by Dessart et al. (2000).

We note that from the measured mean acceleration rate of $\approx$50 km s^{-1} hr^{-1} inferred for the clumps, we predict a "crossing time" of approximately 10.8 hr. This value is larger than the measured 7.5 hr duration of subpeak events. This suggests that the crossing time is somewhat longer than the duration of a subpeak event (which could be explained, e.g., by the clumps being actually destroyed or recycled after $\approx$7.5 hr). However, we have assumed in the degradation function procedure that the acceleration rate was constant over the emission range. Obviously, the emission range for C III λ5696 is large enough that this cannot hold true. It is likely then that the duration of subpeak events has been underestimated, because the motion of subpeaks in ξ space is not linear. Given these uncertainties, the measured minimal duration of subpeak events is close enough to the predicted value (70%) that the hypothesis that clumps have a finite lifetime is only weakly supported by these data.

4.4. *Simulations*

With our model, we produced simulations of spectroscopic time series using the same sampling as the data in order to facilitate the comparison. We produced simulations with various numbers of clumps in the wind, all having equal mass and size and following the general wind velocity law. We have assumed that there was no interclump component, i.e., all the emission comes from the clumps. Under these hypotheses, we find that about $N = 50{,}000$ clumps, on average, must reside in the $700 < V < 1150$ km s^{-1} wind velocity range in order to reproduce the magnitude of the C III λ5696 line profile variations observed in HD 192103. This is consistent with the number of clumps predicted in § 3.4.

Figure 11 shows the emission ranges for three different models (denoted A, B, and C). All three models use the C III emission range derived by Dessart et al. (2000), which we have shown to be consistent with our observations (see § 4.3). Model A also uses the Dessart et al. (2000) emission range for C IV. Models B and C, on the other hand, assume that C IV emission occurs over a more extended range, to a point where the C IV/C III emission ratio increases outward at large distances from the star (model C). This is in contradiction with the general assumption that the C IV/C III ionization ratio monotonically decreases outward in Wolf-Rayet winds. Nevertheless, we show that these extended C IV emission ranges provide better fits to the observed line variability levels.

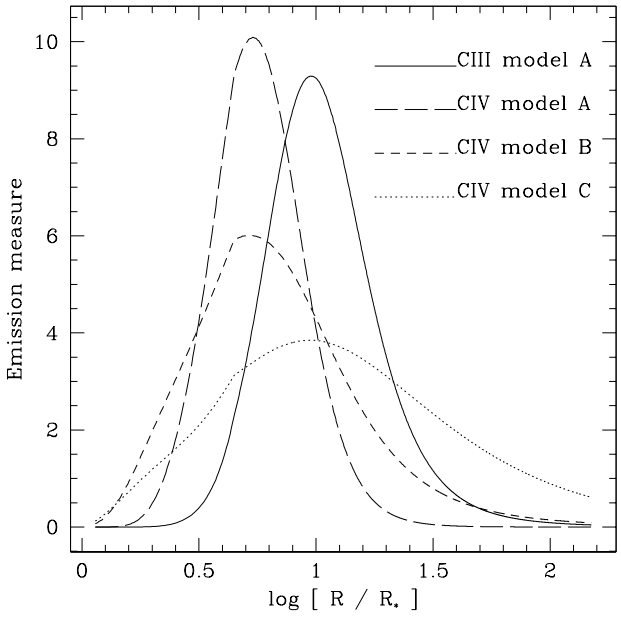

FIG. 11.—Emission range of the C III λ5696 and C IV $\lambda\lambda$5801, 5812 emission lines as used in the simulations. The C IV curve is for the *combined* emission from C IV λ5801 and C IV λ5812. Model A uses the emission ranges derived by Dessart et al. (2000) from spectroscopic modeling of WR 135. Models B and C use the same emission range for C III as in model A but use increasingly larger emission volumes for C IV, which yield lower variability in the C IV emission line. Model C yield variability levels in the C IV line that are most consistent with the observations, but the extended range in C IV emission is apparently inconsistent with an outward ionization stratification of the wind.

The resulting simulations are plotted in Figures 12, 13, and 14. For the C III λ5696 emission line, one can see that both the shape of the line profile and the variability patterns in the simulations reproduce very well the observations. For the C IV doublet, the intensity of the variability levels is clearly reduced as the line emission range increases (from model A to C). The shape of the C IV emission doublet is also reasonably well reproduced, with the best fit provided by model B. The blue edges of the C IV lines are not well reproduced, however, because we have not accounted for P Cygni absorption effects. The fact that model C provides the best fit to the variability levels raises questions about the general hypotheses related to line emission in a clumped wind (see discussion below).

We repeated the cross-correlation analysis (see § 3.5) for the simulations, using the red wing of the C III emission line as the correlation response. Results are shown in Figure 15. We find significant correlations between the C III and C IV variability patterns in all three cases. The amplitude of the correlation is definitely larger for models B and C than for model A, which is consistent with the larger overlaps between the C III and C IV emission ranges in these models.

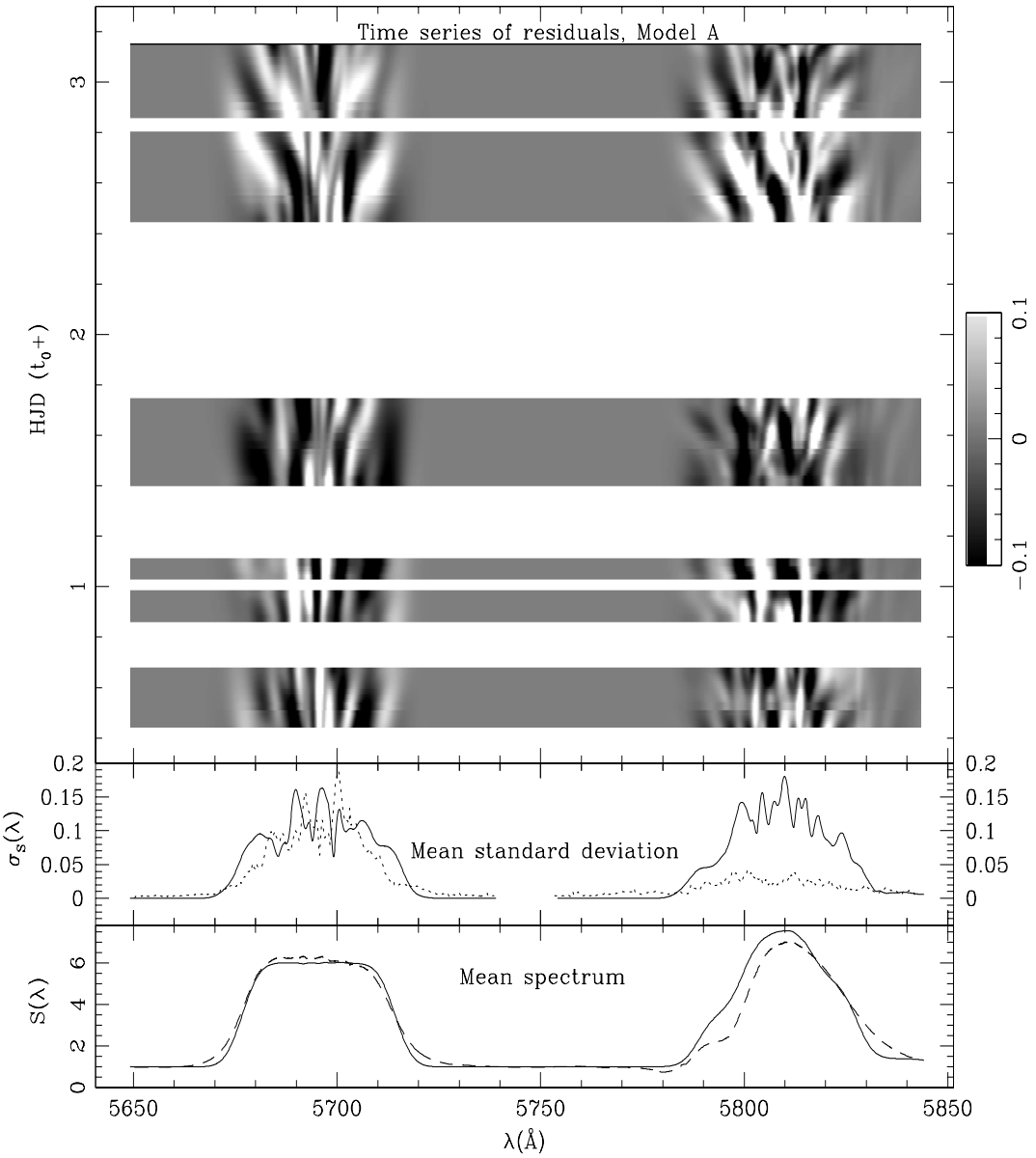

FIG. 12.—Simulation of variability induced in the C III λ5696 line and the C IV λ5808 doublet by a fully clumped, optically thin wind. The range of the C III and C IV emission is based on the model by Dessart et al. (2000). *Bottom panel*: Mean profile plotted with the observed WR 135 spectrum (*dashed line*). *Middle panel*: Mean standard deviation from the simulation compared with the mean standard deviation form the data (*dotted line*). The emission profile and variability levels in the C III λ5696 line are reproduced reasonably well. The P Cygni absorption troughs are not modeled. The variability level in C IV is much higher in the simulations, and the line profile shape is significantly narrower. This suggests problems either with the assumed C IV emission range and/or with the assumption that clumping is uniform throughout the wind.

The fact that we still find a significant correlation between C III and C IV in model A confirms that a correlation between the LPV patterns can be measured as long as there is some overlap between the line emission regions.

5. DISCUSSION

The variability patterns observed in the optical emission lines of WR stars can be easily explained if we assume (1) that the wind is inhomogeneous, (2) that the bulk of the line emission occurs in a spherical shell of finite thickness, and (3) that the inhomogeneities are being accelerated away from the star.

The spectroscopic data presented in this paper clearly demonstrate that clumping in WR stars does not occur in shells of compressed material but rather in a collection of small, discrete overdensities. It is not possible to determine the exact inhomogeneous structure of the wind at this point. The two most likely possibilities are (1) clumps immersed in a relatively dense interclump medium, and (2) full-scale clumping, i.e., the whole wind is basically made up of clumps, with negligible interclump medium. The very large growth factors derived for radiative line-driven instabilities (Gayley & Owocki 1995) favors the hypothesis of very dense clumps with a very tenuous interclump medium. The huge number of clumps inferred from our simulations implies that instabilities would be very localized and would occur on small scales, as opposed to large-scale instabilities involving the compression in a single shock front of a large fraction of the ejected material. Localized clumps are consistent with radiative instabilities as the source of the inho-

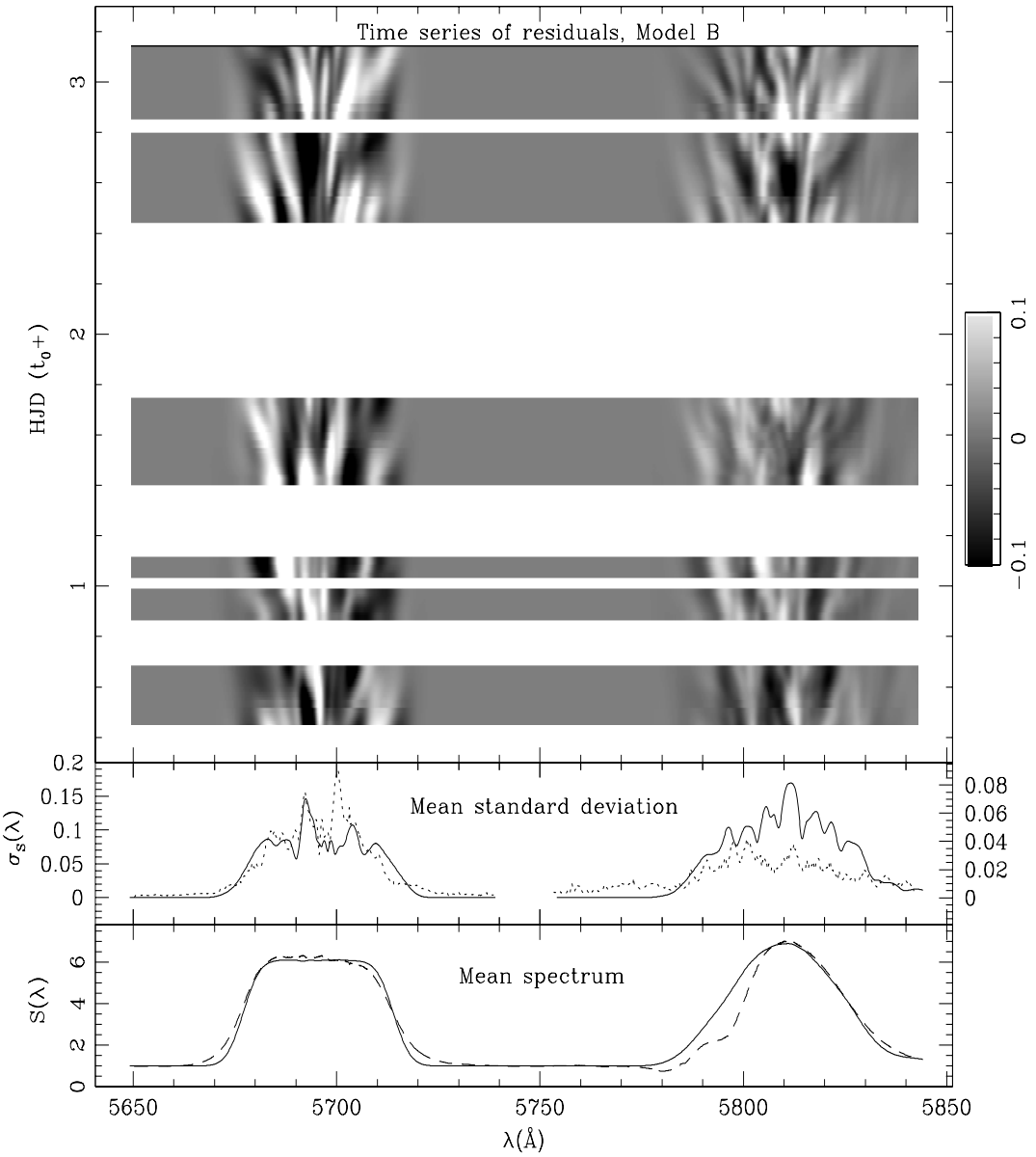

FIG. 13.—Same as Fig. 12, but for a model in which the C IV line emission occurs farther out in the wind, with a larger overlap on the C III emission volume. Both the C III and C IV line profiles from the simulations reproduce very well the observed WR 135 line profiles. The variability levels in C IV are now smaller than for model A (see Fig. 12), although they are still significantly larger than the observed variability levels. The lower variability levels arise because the C IV emission volume is larger, and therefore more clumps are involved in the C IV line emission.

mogeneities. However, it is still unclear whether or not radiation line-driving is the main source of acceleration in WR winds (Puls, Springmann, & Lennon 2000).

Current spectral modeling at least suggests clumping factors $f \sim 0.1$ (Hillier & Miller 1999), which basically means that clumps would occupy about 1/10 of the overall wind volume. (The use of a "clumping factor" is, however, an oversimplification of the problem, reducing clumping to a single parameter, and interpretations should be made with caution.) The very large numbers of clumps inferred from our analyses ($N \gtrsim 10^4$) imply that individual clumps must be relatively small. This model of inhomogeneities as a large collection of small components is supported by the photometry, which reveals very little variation in the global WR luminosity at the time spectroscopic observations were made.

Assuming the C III emission volume to fill up an $r = 32\ R_*$ sphere centered on the star, and assuming the coexistence within that volume of 7×10^4 clumps with a filling factor $f = 0.1$, then individual clumps would have typical radii of about $r_{\rm clump} = 0.4\ R_*$, i.e., about 1/10 of the stellar core radii (this is to be regarded as a very rough estimate, given the oversimplification introduced by the theoretical "filling factor"). Of course, for the filling factor to remain constant throughout the wind, the clumps would need to expand as they propagate away from the star, which means that near the stellar core they would be denser but also much smaller.

The simplest explanation for the variability in the emission line is statistical fluctuations in the number of emitting clumps. This is consistent with the observation that the line profile variations in WR 135 are stochastic in nature. One

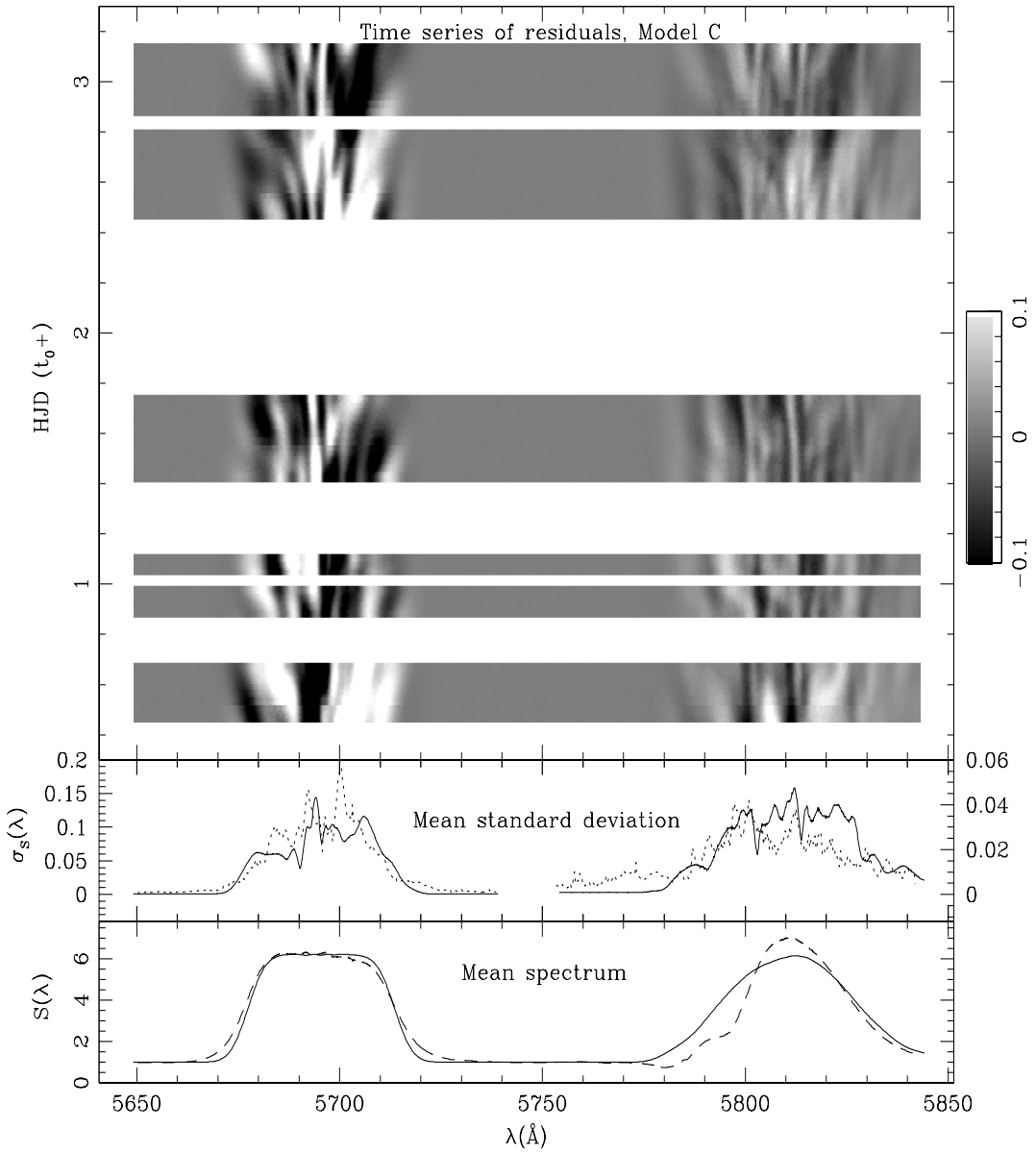

FIG. 14.—Same as Figs. 12 and 13 but for a model in which the emission volume is much larger. This yields better agreement with the data for the line profile variability levels in C III and C IV. However, the C IV line profile is now broader than the observed WR 135 profile. This discrepancy indicates than the low variability levels in the C IV doublet cannot entirely be accounted for by a larger emission volume for C IV. This suggests that wind clumping is increasing with distance from the star and that C IV variability is lower than in C III in part because C IV is formed closer to the star.

important consequence of this model is that, since the relative variability is inversely proportional to the square root of the mean number of clumps which contribute to the emission, the variability in a given emission line depends on the size of the emitting volume for that line. For a given velocity, we can estimate the number of clumps at a given location in the wind or, more appropriately, the expected number of clumps in a given velocity range.

Let $n_v(v)$ be the mean number of clumps within a given velocity range $[v, v + dv]$. If we assume that clumps are ejected through the wind at a steady rate, then we have $n_t\,dt = n_v(v)dv$, where n_t is a constant. Hence we find that $n_v(v) = n_t(dv/dt)^{-1}$, or simply that $n_v(v) \sim a(v)^{-1}$, where $a(v)$ is the radial wind acceleration as a function of the wind velocity. We plot $n_v(v)$ in Figure 16, for the velocity law that we used in our simulations (see § 4.1). One sees that the relative number density of clumps grows very quickly past about $v = 1000$ km s^{-1}. We believe that this probably contributes to the lower observed variability levels near the edges of the C III λ5696 emission line in WR 135 (see § 3.2). We predict that WR emission lines which are formed in regions where the wind has almost reached its terminal velocity should show very little variability. The most variable emission lines should be those which are formed relatively close to the star in a relatively thin shell.

In this respect, the fact that we observe a larger variability in the C III line than in the C IV line is problematic, since we would expect a priori that the C IV emission volume would be smaller, since this line is formed closer to the star. Our simulations apparently suggest that C IV is strongly overlapping with C III and that significant C IV emission occurs farther out in the wind than C III. This is in contra-

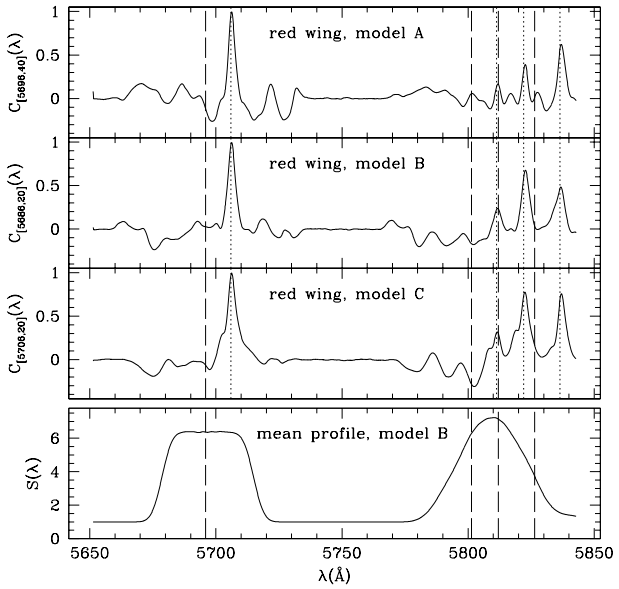

FIG. 15.—Cross-correlation analysis for the variable patterns from the simulations, performed in the same way as the cross correlation analysis of the observations (compare with Fig. 7). Clear correlations appear in the C III–C IV λ5808 blend. The red wing of the C III λ5696 emission line (5696 Å < λ < 5716 Å) is used as the reference. The correlation with the C IV lines is greater in models B and C, consistent with the larger overlap in the C III and C IV emission zones in these models.

diction with several other lines of observational evidence which all support the idea that C IV is formed closer to the star than C III (Willis 1982).

There are three possible explanations for the larger variability in C III which would at the same time be consistent with C III being formed farther out in the wind than C IV.

1. Clumping in the wind increases with distance from the star. The higher variability in C III λ5696 is then explained by the wind becoming fully clumped in that range, whereas the wind would still be relatively more homogeneous where C IV arises. In any case, observed variability in the polarization of Wolf-Rayet stars implies that clumping must at least be initiated deep in the photosphere, since the formation of clumps farther than $\tau = 1$ cannot produce the observed variable polarization of WR winds (Brown et al. 1995).

2. Opacity effects may be important in the C IV emission, reducing the variability in the line due to clumping. This would be especially important if there exists, e.g., a hierarchy of clumps with different masses and density. Dense, massive clumps would be very bright relative to their surroundings in the optically thin case and would contribute significantly to the line-profile variability. In the optically thick case, on the other hand, these dense, massive clumps would not be fainter when optically thick and may be as effective in producing line-profile variations.

3. The effective C III λ5696 emission volume may be smaller for a given emission range in wind velocity space. This could occur if, for example, C III λ5696 emission depends on very specific conditions of clump density, pressure, and temperature, such that not all wind clumps at a given distance from the star would be emitters. The large variability in the C III emission line would be a consequence of the smaller number of clumps involved in the emission at any given time.

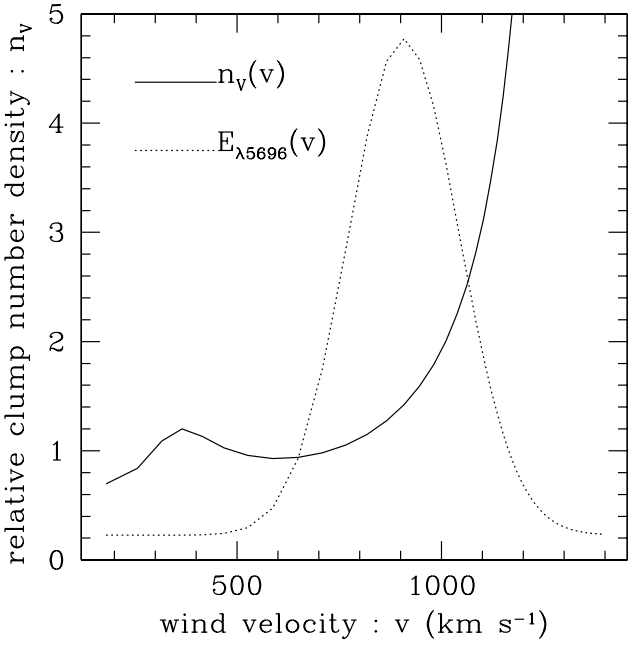

FIG. 16.—Relative number density n_v of wind clumps as a function of the bulk wind expansion velocity v relative to the star. The wind is accelerated up to a certain distance from the star, where it asymptotically approaches some terminal velocity. As a result, the number of clumps per velocity interval increases rapidly toward the wind terminal velocity. Because line variability is inversely proportional to the square root of the number of clumps ($\sigma \sim n_v^{-1/2}$), it is expected to decrease as emission occurs in larger velocity intervals. This effect explains the lower observed variability levels near the edges of the C III λ5696 line (see Fig. 3).

The hypothesis that the emission occurs in a shell of finite thickness centered on the star provides a straightforward interpretation for the transient nature of the variable subpeaks: the duration of a given subpeak event actually corresponds to the time it takes for a clump to move across the C III λ5696 emission shell (the crossing time). An alternate interpretation would be that the duration of subpeak events corresponds to an actual cycle of creation and destruction (lifetime) of a clump in the wind. But since the observed duration of subpeak events is on the order of the expected crossing time, the latter interpretation appears to be contrived. Independent data to support the idea of a finite lifetime for wind clumps is required to confirm this hypothesis. One way to test for this possibility would be to look for subpeak events in all spectral emission lines, until it can be shown unambiguously that the subpeak duration in one line is clearly shorter than the expected crossing time. Alternatively, one could look for evidence for the propagation of clumps from one region of high ionization (closer to the star) to a region of lower ionization (farther from the star). Persistence of subpeak features in several ionization zones, i.e., at different distance ranges from the star, would then rule out the hypothesis of a finite lifetime. This may be possible by comparing spectroscopic time series of two lines of different ionization potential and showing that their variability patterns correlate (although with a certain time delay).

The correlation observed between the LPV patterns of C III λ5696 and C IV λ5812 (§ 3.5) implies that their respective emission volumes have a significant overlap. Unfortunately, it is not possible at this point to obtain a reliable estimate for the magnitude of these overlaps. Although the simulations clearly show an increase in the correlation

when the overlapping volume is increased, this effect is not easily quantified. Comparison with the correlation obtained from the data is not reliable because the amplitude of the correlation is affected by instrumental noise. Quantification of the overlap might be possible, however, if one could obtain extended times series ($N > 1000$ spectra) of pairs of variable line profiles with extremely high signal-to-noise ratio (S/N > 500).

Results from our cross-correlation technique also nicely demonstrate that LPV patterns can actually be used to resolve the components of a WR emission blend. This is possible because the width of the individual variable subpeaks in LPV patterns is relatively small ($\simeq 100$ km s^{-1}) compared to the full width of the emission lines themselves (> 1000 km s^{-1}). The only requirement is that the emission lines must have overlapping emission volumes, such that they have similar intrinsic LPV patterns. High-resolution, high signal-to-noise ratio time series of Wolf-Rayet spectra can thus be used to deblend emission line doublets/multiplets and detect unsuspected emission components. This might prove to be very useful, e.g., for Wolf-Rayet stars with very fast ($v > 1500$ km s^{-1}) winds whose emission lines tend to be severely blended.

6. CONCLUSIONS

We have presented extensive high signal-to-noise ratio spectroscopic time series of the Wolf-Rayet star HD 192103, revealing variability patterns in the C III λ5696 and C IV λ5808 wind emission lines. The variability patterns consist of a number of narrow, transient emission subpeaks which tend to move toward the nearest line edge.

Photometric observations were carried out simultaneously and revealed the star to be photometrically quiet down to the 0.01 mag level. This strongly suggests that the global wind geometry remained very stable during the spectroscopic observations and that the variability in the emission lines very likely results from local perturbations in the wind (small-scale clumping).

We have successfully reproduced the patterns of line variability using a model in which the wind is assumed to consist of a very large number of relatively small clumps. The subpeak motion in a direction from line center to line edge requires the clumps to be radially accelerated away from the star. The transient nature of the variable subpeaks requires the bulk of the line emission to occur within a shell of finite thickness. The duration of subpeak events is roughly consistent with the time it takes for a clump to cross the line emission region. However, there is some indication that the clumps might be evolving, since the duration of subpeaks events appears to be a little smaller that the expected crossing time.

The general variable behavior is interpreted as a statistical process, related to the finite number of clumps that contribute to the line emission at a given time. We observe that the λ5801 and λ5812 components of the C IV λ5808 doublet are about 4 times less variable than the C III λ5696 emission line. We propose that this is due to the fact that, based on Poisson statistics, fewer clumps are responsible for the C III emission than for C IV. According to our model, this is possible if the C IV emission volume is larger than that for C III λ5696. Although it is possible that some C IV emission occurs at large distance from the star, a more likely explanation is that clumping increases with distance from the star (whereas our model assumes uniform clumping levels throughout the wind). Hence, the C III emission line, formed farther out than C IV, would be more variable because of larger wind clumping in that part of the wind. Alternately, opacity effects in C IV could also attenuate the variability due to clumping in that line, if the C IV emission is not optically thin.

We find a significant correlation between the LPV patterns in C III λ5696 and in C IV λ5812. This implies that, although these lines are not formed at exactly the same range in the wind, there is at least a significant overlap in their emission volume.

We also find a correlation response between the LPV patterns in C III λ5696 and a range of wavelengths that match with the expected location of the C III λ5826 emission. We argue that this latter line must be a relatively weak component of the λ5808 line complex, but that its variability pattern is easily detected because C III λ5826 is more variable than the C IV components. Hence, cross-correlation analysis of LPV patterns is revealed as an effective tool to resolve the components in WR line emission blends.

We suggest that significant advances can be made by simultaneously monitoring WR emission lines of different ionization species. By using the analysis methods described in this paper, it should then be possible to use the variability patterns in the emission lines to (1) constrain the size and location of the line-emission regions, (2) investigate the ionization stratification, (3) provide critical constraints on the wind dynamics by directly measuring the wind acceleration at different distances from the star, and (4) determine the magnitude of wind clumping at different distances from the star. These new pieces of information, combined with constraints from spectral analysis models, could be the key to determining the structure of Wolf-Rayet winds in a self-consistent way.

S. L. acknowledges the support provided by a postdoctoral fellowship from NSERC (Canada). A. F. J. M. and N. SL. are also grateful to NSERC (Canada) and FCAR (Québec) for financial assistance.

REFERENCES

Brandi, E., Ferrer, O. E., & Sahade, J. 1989, ApJ, 340, 1091
Brown, J. C., Richardson, L. L., Antokhin, I., Robert, C., Moffat, A. F. J., & St-Louis, N. 1993, A&A, 295, 725
Dessart, L., Crowther, P. A., Hillier, D. J., Willis, A. J., Morris, P. W., & van der Hucht, K. A. 2000, MNRAS, 315, 407
Eenens, P. R. J., & Williams, P. M. 1994, MNRAS, 269, 1082
Eversberg, T., Lépine S., & Moffat, A. F. J. 1998, ApJ, 494, 799
Gayley, K. G., & Owocki, S. P. 1995, ApJ, 446, 801
Gayley, K. G., Owocki, S. P., & Cranmer, S. R. 1995, ApJ, 442, 296
Hamann, W. R., & Koesterke, L. 1998, A&A, 335, 1003
Hamann, W. R., Leuenhagen, U., Koesterke, L., & Wessolowski, U. 1992, A&A, 281, 184
Herald, J. E., Schulte-Ladbeck, R. E., Eenens, P. R. J., & Morris, P. 2000, ApJS, 126, 469
Hillier, D. J. 1991, A&A, 247, 455
Hillier, D. J., & Miller, D. L. 1999, ApJ, 519, 354
Ignace, R., Brown, J. C., Richardson, L. L., & Cassinelli, J. P. 1998, A&A, 330, 253
Koesterke, L., & Hamann, W.-R. 1995, A&A, 299, 503
Kostenko, F. V., & Kholtygin, A. F. 1999, Astrophysics, 42, 280
Lamers, H. J. G. L. M. 1994, Ap&SS, 221, 41
Lépine, S. 1996, in WR Stars in the Framework of Stellar Evolution, ed. J.-M. Vreux et al. (33d Liège Int. Astrophys. Colloq.) (Liège: Université de Liège, Inst. d'Astrophysique), 253

Lépine, S., Eversberg, T., & Moffat, A. F. J. 1999, AJ, 117, 1441 (Paper III)
Lépine, S., & Moffat, A. F. J. 1999, ApJ, 514, 909 (Paper II)
Lépine, S., Moffat, A. F. J., & Henriksen, R. N. 1996, ApJ, 466, 392
Lépine, S., et al. 2000, in preparation
Luehrs, S. 1997, PASP, 109, 504
Maeda, Y., Koyama, K., Yokogawa, J., & Skinner, S. 1999, ApJ, 510, 967
Moffat, A. F. J. 1996, in Wolf-Rayet Stars in the Framework of Stellar Evolution, ed. J. M. Vreux, A. Detal, D. Fraipont-Caro, E. Gosset, & G. Rauw (Liège: Université de Liège, Institut d'Astrophysique), 199
Moffat, A. F. J., & Marchenko, S. V. 1996, A&A, 305, L29
Moffat, A. F. J., et al. 1998, ApJ, 497, 896
Morel, T., St-Louis, N., Moffat, A. F. J., Cardona, O., Koenigsberger, G., & Hill, G. M. 1998, ApJ, 498, 413
Moffat, A. F. J., & Robert, C. 1991, in IAU Symp. 143, Wolf-Rayet Stars and Interrelations with Other Massive Stars in Galaxies, K. A. van der Hucht (Dordrecht: Kluwer), 109
Morel, T., et al. 1999, ApJ, 518, 428
Morris, P. W., van der Hucht, K. A., Crowther, P. A., Hillier, D. J., Dessart, L., Williams, P. M., & Willis, A. J. 2000, A&A, 353, 624
Nugis, T. 1994, Ap&SS, 221, 217
Nugis, T., Crowther, P. A., & Willis, A. J. 1998, A&A, 333, 956
Prinja, R. K., Barlow, M. J., & Howarth I. D. 1990, ApJ, 383, 466
Puls, J., Springmann, U., & Lennon, M. 2000, A&AS, 141, 23
Rochowicz, K. 1997, Acta Astron., 47, 381
Smith, P. L., Heise, C., Esmond, J. R., & Kurucz, R. L. 1995, Kurucz CD-ROM 23, Atomic Spectral Line Database (Cambridge: SAO)
Springmann, U. 1994, A&A, 289, 505
St-Louis, N., Moffat, A. F. J., Lapointe, L., Efimov, Yu. S., Shakhovskoy, N. M., Fox, G. K., & Piirola, V. 1993, ApJ, 410, 342
Willis, A. 1982, MNRAS, 198, 897
Young, A. T., et al. 1991, PASP, 103, 221